Contents lists available at ScienceDirect

Microporous and Mesoporous Materials

Preparation of hierarchical SAPO-18 via alkaline/acid etching

Dong Fan [a,1], Yuyan Qiao [b,1], Kaipeng Cao [a,c], Lijing Sun [a,c], Shutao Xu [a], Peng Tian [a,**], Zhongmin Liu [a,*]

[a] National Engineering Laboratory for Methanol to Olefins, Dalian National Laboratory for Clean Energy, Dalian Institute of Chemical Physics, Chinese Academy of Sciences, Dalian, 116023, China
[b] China Chemical Technology Research Institute, China National Chemical Engineering Co., Ltd (CNCEC), Beijing, 100007, China
[c] University of Chinese Academy of Sciences, Chinese Academy of Sciences, Beijing, 100049, China

ARTICLE INFO

ABSTRACT

Hierarchical SAPO-18 molecular sieve was successfully post-synthesized in the alkaline tetraethyl ammonium hydroxide (TEAOH) solution and hydrochloride (HCl) acid solution. In the TEAOH solution, preferential dissolution occurs surrounding the defect sites in a controlled manner, leading to hierarchical SAPO-18 with well-preserved chemical compositions and crystallinities. In acidic solution, the dissolution is revealed to be sensitive to both the defects and the chemical compositions (selective dissolution of the Si-O-Al domains), which cooperatively contribute to the generation of meso-/macropores in the crystals. The crystallization of SAPO-18 precursor is thus inferred to proceed via an oriented nanoparticle attachment mechanism in the early stage. The twinning and intergrowth of nanoparticles occur in an ordered way, leading to the oriented arrangement of the crystallite boundaries. The defects located at the intergrowth interface are prone to acid/alkaline attacks, and play crucial role in the development of hierarchical pore systems. The hierarchical SAPO-18 sample exhibits excellent catalytic reaction performance in the liquid phase benzylation reaction of benzene and benzyl alcohol.

1. Introduction

Molecular sieves are a kind of crystalline materials of uniform pores/channels and 3-dimensional frameworks, which find wide applications in various fields as adsorbents, ion-exchangers and catalysts, mainly due to their shape-selective properties [1–4]. Molecular sieves are endowed with the unique shape-selectivity due to their confined microporous structures of molecular dimensions. However, the innate micropore channels could alternatively lead to significant transport limitations, seriously restricting their applications.

Great efforts have been devoted to improving the transport properties of molecular sieves, focusing on the tailoring of their morphologies. Various strategies have been developed, among which hierarchical zeolite is one of the most attractive approaches [5]. The essence of hierarchical zeolite is to introduce auxiliary larger porosities into original native micropore system. The synthesis strategies of hierarchical zeolites could be generally classified into two categories: the direct synthesis method (bottom-up strategy) and the post-synthetic method (top-down

strategy) [6–9]. The former strategy involves the direct bottom-up synthesis of hierarchical zeolite, frequently with the assistance of hard/soft template. Jacobsen et al. prepared hierarchical ZSM-5 single crystals, using nano-sized carbon black particles as the sacrificial mesopore agent [10]. Previously, our group also succeeded in the preparation of mesoporous MOR, Beta and SAPO-34 molecular sieves by using surfactants, cationic polymers or organic silanes as mesoporogens [11–14]. However, the mesoporogens could only function in very limited and rigorous conditions. And the high cost of the mesoporogens restricts the massive applications of the templated synthesis of hierarchical zeolites.

Post-synthesis treatment, *e.g.* acid leaching or alkaline treatment, is a more cost-effective modification route to tailor the compositional and textural properties of zeolites. In effect, dealumination by acid leaching or steaming treatment is a practical method employed to enhance the Si/Al ratios of aluminosilicate zeolites [15]. Desilication in alkaline was extensively investigated to introduce mesoporosity into the zeolites [16]. Groen et al. created uniform intracrystalline mesopores inside

---

ZSM-5 molecular sieves using NaOH post-synthetic treatment [17,18]. Under suitable conditions, the same group also succeeded in the preparation of mesoporous zeolites with BEA, MOR and FER topologies [19,20]. Verboekend et al. also treated a series of aluminophosphate molecular sieves, including AlPO-5, SAPO-5, SAPO-11 and SAPO-34, by various acids and bases. They found that the composition of the parent molecular sieve is vital for the treatment results [21]. Based on controlled alkaline/acid leaching strategy, we recently reported the successful preparation of hollow SAPO-34 single crystals [22]. However, due to the low stability of SAPOs in alkaline and acid solutions, research on alkaline treatment and acid treatment of SAPO molecular sieves is still rather limited.

In this contribution, SAPO-18 was selected for the first time to undergo alkaline and acid treatments. TEAOH, sodium hydroxide (NaOH), HCl and oxalic acid ($H_2C_2O_4$) solutions were employed as treatment mediums. The effects of different acid/alkaline mediums were investigated and compared. Mesopores and/or macropores were successfully introduced into the SAPO-18 crystals, and the rationale behind the variation of morphologies and compositions was discussed.

2. Experimental

2.1. Preparation of the SAPO-18 precursor

The SAPO-18 precursor was hydrothermally synthesized using N, N-diisopropyldiethylamine (DIEA) as the organic template. The molar ratio of the initial gel was DIEA: Al_2O_3: P_2O_5: SiO_2: $H_2O = 1.8$: 1.0: 1.0: 0.4: 50. The detailed preparation procedure is as follows: deionized water, pseudoboehmite, H_3PO_4 (85 wt%), tetraethyl orthosilicate (TEOS), and DIEA were sequentially added into a beaker, and the resultant mixture was stirred at room temperature for 3 min until homogeneity. Afterwards, the mixture was transferred into an autoclave, placed in the oven and crystallized at 160 °C for 48 h under tumbling conditions. The solid product was washed, centrifuged and dried at 110 °C for 12 h. To clarify, the prepared precursor SAPO-18 sample is denoted SP18-P.

2.2. The procedures for acid/base treatment

All the alkaline or acid treatment conditions are listed in Table 1. The typical alkaline treatment process in TEAOH solution was as follows: 1 g of the SAPO-18 precursor was added to 50 ml of 0.1 M TEAOH solution. Then the mixture was mixed and heated at 80 °C for 30 min. The treated sample was washed with deionized water, recovered through centrifugation and dried at 110 °C for 12 h. The obtained sample was named SP18-TEAOH-0.1, with TEAOH indicating the treatment solution and 0.1 indicating its molar concentration. Similar treatment procedures and naming rules also apply to other samples listed in Table 1.

2.3. Catalyst characterization

The Powder X-ray diffraction (XRD) patterns of the synthesized samples were recorded using PANalytical X'Pert PRO X-ray diffractometer with Cu Kα radiation ($\lambda = 0.154059$ Å) at 40 kV and 40 mA from 5° to 50°. The scanning electron microscope (SEM) images of the synthesized samples were recorded on a Hitachi SU8020 SEM equipment. Transmission electron microscopy (TEM) images were recorded with a JEM-2100 electron microscope. The bulk and surface compositions of samples were determined with Philips Magix-601 X-ray fluorescence (XRF) spectrometer and VG ESCALAB MK2 X-ray photoelectron spectrometer (XPS). N_2 adsorption and desorption measurements were tested on a Micromeritics ASAP 2020 analyzer. The total surface area was calculated by the BET method. The micropore volume and area were calculated by t-plot method. The pore distribution for mesopore and macropore ranges was analyzed using mercury intrusion porosimetry at room temperature on a Micromeritics AutoPore IV 9510 Mercury

Table 1

Post treatment conditions, relative crystallinities and products yields of the samples.

Sample[a]	reagent	C (M)	SLR[b] (g/L^{-1})	Relative Crystallinity[c]	Product Yield
SP18-TEAOH-0.1	TEAOH	0.1	20	95%	76%
SP18-TEAOH-0.2	TEAOH	0.2	20	98%	64%
SP18-TEAOH-0.4	TEAOH	0.4	20	93%	40%
SP18-NaOH-0.1	NaOH	0.1	20	87%	82%
SP18-NaOH-0.2	NaOH	0.2	20	60%	70%
SP18-NaOH-0.4	NaOH	0.4	20	26%	69%
SP18-$H_2C_2O_4$-0.05	$H_2C_2O_4$	0.05	20	90%	84%
SP18-$H_2C_2O_4$-0.1	$H_2C_2O_4$	0.1	20	69%	66%
SP18-$H_2C_2O_4$-0.2	$H_2C_2O_4$	0.2	20	35%	49%
SP18-HCl-0.05	HCl	0.05	20	88%	85%
SP18-HCl-0.1	HCl	0.1	20	95%	75%
SP18-HCl-0.2	HCl	0.2	20	77%	56%

[a] All the alkaline/acid treatments are carried out at 80 °C for 30 min.
[b] Solid-to-liquid ratio: weight of SAPO-18 per liter of treatment solution.
[c] The relative crystallinity is calculated based on the relative intensity of the strongest peak at around 9.5° (2 theta); define the relative crystallinity of parent SAPO-18 as 100%.

Intrusion Porosimeter. All the solid-state NMR experiments were performed on a Bruker AvanceIII 600 spectrometer equipped with a 14.1 T wide-bore magnet. The resonance frequencies were 156.4, 242.9 and 119.2 MHz for ^{27}Al, ^{31}P and ^{29}Si, respectively. Chemical shifts were referenced to 1.0 M $Al(NO_3)_3$ for ^{27}Al, 85% H_3PO_4 for ^{31}P, and 2,2-dimethyl-2-silapentane-5-sulfonate sodium salt (DSS) for ^{29}Si. ^{27}Al and ^{31}P MAS NMR experiments were performed on a 4 mm MAS probe with a spinning rate of 12 kHz. ^{27}Al MAS NMR spectra were recorded using one pulse sequence. A 200 scans was accumulated with a π/8 pulse width of 0.75 μs and a 2 s recycle delay. ^{31}P MAS NMR spectra were recorded using high-power proton decoupling. A 32 scans was accumulated with a π/4 pulse width of 2.25 μs and a 30 s recycle delay. ^{29}Si MAS NMR spectra were recorded with a 4 mm MAS probe with a spinning rate of 8 kHz. A 4096 scans was accumulated with a contact time of 3 ms and a recycle delay of 2 s. The temperature-programmed desorption of ammonia (NH$_3$-TPD) was carried out with an Autochem 2920 equipment (Micromeritics). The calcined samples (100 mg, 40–60 mesh) was activated at 650 °C for 60 min (10 °C/min) in He, and then cooled down and saturated with ammonia at 150 °C for 30 min. After the samples were purged with He (30 ml/min) for 30 min, the measurements of the desorbed NH$_3$ were performed from 150 to 650 °C (10 °C/min) under He (30 ml/min).

2.4. Catalytic testing

Alkylation of benzene with benzyl alcohol was performed in a Parr autoclave. 0.25 g of the catalyst was transferred into the 100 ml Parr reactor. Then 29.8 g benzene (99.5%) and 0.52 g benzyl alcohol (98%) were added in sequence resulting in a molar ratio of benzene to benzyl alcohol of 80. The reactor was purged with nitrogen and maintained a permanent pressure of 20–25 bars during the reaction, in order that the

reactants could keep in the liquid phase at the reaction temperature of 170 °C. The mixture was stirred at 300 rpm throughout the run, which was determined to be sufficiently fast. After 1 h reaction, a small amount of liquid sample was withdrawn and analyzed by using GC–MS equipped with a capillary HP-5 (Agilent Technologies) column.

3. Result and discussion

3.1. XRD analysis

The XRD patterns of the samples before and after alkaline and acid treatments are presented in Fig. S1. Well-resolved diffraction pattern typical for AEI structure can be observed for SAPO-18 precursor (sample SP18-P). No obvious intensity decrease is observed after treatment in TEAOH solution, irrespective of the TEAOH concentration (0.1–0.4 mol/L) employed, implying the well-kept AEI structure of the samples. In contrast, the diffraction intensity drops sharply even in NaOH solution of merely 0.1 mol/L, corresponding to framework degradation. This demonstrates a clear difference of the treatment efficacies of the inorganic and organic alkaline solutions. The parent sample SP18-P used in this study is in effect in its as-synthesized form, without the calcination removal of organic templates, which could prevent the relatively bulky TEA^+ cations and the accompanying OH^- anions from entering and interacting with the internal structure. Consequently, the TEAOH solution could only gradually dissolve the outer surface, preserving the internal structure and crystallinity from degradation. In NaOH solution, the transport of the small Na^+ cations is barely influenced by the encapsulated template molecules and the OH^- anions are hence free to enter the cages of SAPO-18 and cause a more severe damage to its internal structure. With the increase of NaOH concentration, the OH^- concentration inside the SAPO-18 channels would have a corresponding increase and the internal structure is more seriously damaged. Table 1 lists the solid yields of the products after different treatments. Compared with TEAOH treatment, the solid yield decreases more slowly with the increase of the alkaline concentration under NaOH treatment. It is

inferred that the sodium cations may coagulate with the amorphous species formed in the dissolution process and contribute to the yield of the solid products.

The post-treatment of SAPO-18 molecular sieves in acid medium is also investigated. After treatment in HCl acid, the crystallinity of all the samples decreases to certain extent and the lowest crystallinity of 77% was observed on SP18-HCl-0.2. However, it should be noted that the crystallinity decrease is not that severe even for SP18-HCl-0.2, suggesting that HCl solution did not lead to serious damage to the framework of SAPO-18. In oxalic acid medium, the framework can be well preserved at low concentration. With the increase of oxalic acid concentration, the crystallinity of the treated sample shows a dramatic drop, implying the damage of the structure. It is speculated that the strong coordination effect of $C_2O_4^{2-}$ group might contribute to the framework degradation. The solid yields of the products shown in Table 1 presents a gradual decrease following the increase of the acid concentration. The relatively low solid yield observed for oxalic acid-treated samples also confirms that oxalic acid interacts stronger with the framework than HCl acid.

3.2. Morphology analysis

The SEM and TEM images of the samples are presented in Fig. 1. The SAPO-18 precursor comprises cubic crystals of around 2 μm. The crystal surface is not smooth with many steps on it. Further grinding the precursor crystals to expose their internal structure, it is interesting to find that the crystals are not solid and their interiors are composed of nanosized crystallites. After treatment in TEAOH solution (0.1 M), radiated pores of meso- and macroscale penetrating into the center of the crystals were created, showing the creation of hierarchical porosity. TEM image reveals that the internal parts of the TEAOH-treated crystals are brighter than the outer part, which suggests that the internal part of the crystals are more easily dissolved. For sample SP18-TEAOH-0.2 treated in 0.2 M TEAOH solution, an enhanced dissolution of the inner part of the crystals could be observed with increased quantities of hierarchical porosities.
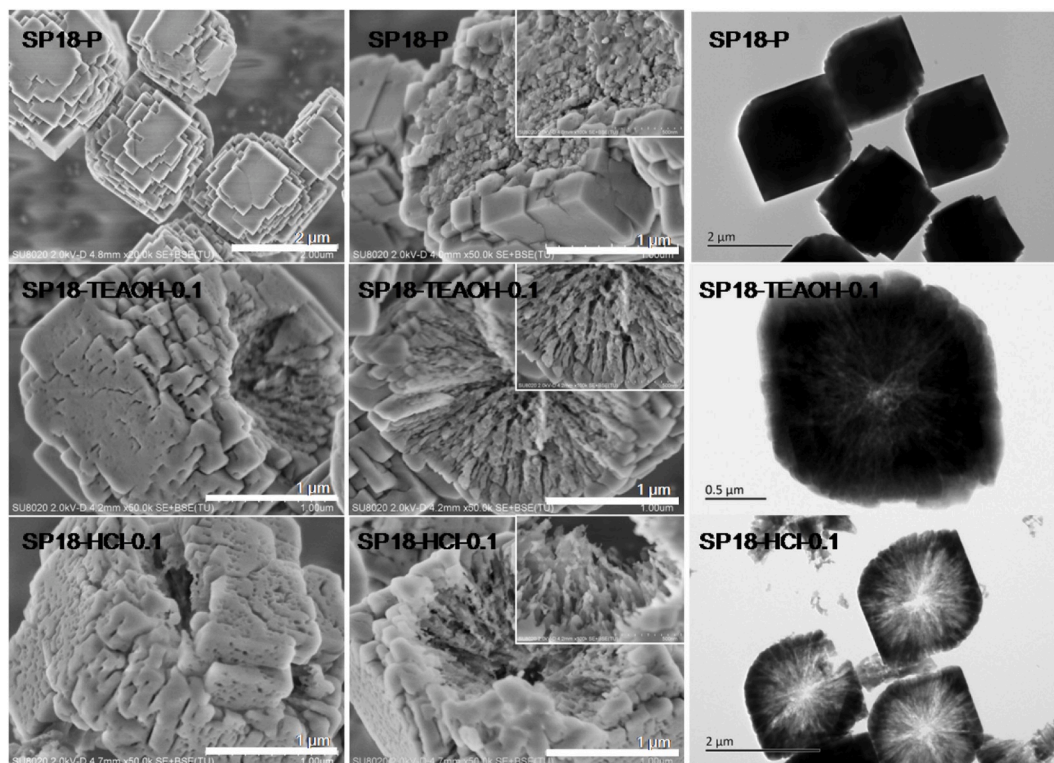
Fig. 1. SEM and TEM images of SAPO-18 precursor and products after alkaline and acid treatments.

For sample SP18-HCl-0.1 treated in HCl solution (0.1 M), the surface of the crystals becomes coarser and more holes are created in the crystals than those after TEAOH treatment. In addition, the edges and corners of the crystals become less demarcated. Some crystals are no longer intact after HCl treatment. All these phenomena demonstrate that HCl interacts strongly with the SAPO-18 precursor. From the TEM image of SP18-HCl-0.1, it is clear that the central part of the crystals was preferentially dissolved during HCl treatment and the dissolution effect is even stronger than TEAOH solution, resulting in the creation of hollow structures inside the crystals. Increasing the concentration of the HCl solution to 0.2 M, the crystal morphology of SP18-HCl-0.2 resembles SP18-HCl-0.1, except for a more severe dissolution of the precursor crystals. Similar morphologies are observed in the case of oxalic acid treatment, indicating similar interactions between SAPO-18 precursor and inorganic HCl and organic $H_2C_2O_4$ acid.

3.3. Compositional analysis

Table 2 shows the bulk and surface compositions of the products after alkali and acid treatments. The Si content on the surface of the SAPO-18 precursor is slightly lower than that in the bulk phase, suggesting that the precursor has a relatively uniform Si distribution. Upon treatment with TEAOH solution of different concentrations, no obvious changes were observed on the bulk and surface compositions. This suggests that the TEAOH solution could uniformly remove the framework elements. When using NaOH solution as the alkaline medium, the relative Si and Al contents increase gradually, while the P content decreases. This phenomenon may be related to the stronger alkalinity of NaOH solution. The OH^- groups of NaOH solution tend to attack the positively charged PO_4^+ in the framework, and hence more P species are removed from the framework. The bulk and surface Si contents significantly decreased after oxalic treatment (0.034 for SP18-$H_2C_2O_4$-0.2), suggesting that oxalate acid preferentially extracts the Si atoms in the framework. The decrease of the Si content is not so evident in HCl acid comparing to that of oxalate acid treatment, suggesting a relatively mild interaction of inorganic HCl solution with the SAPO-18 precursor.

3.4. Textural analysis

The N_2 adsorption-desorption isotherms and the BJH pore size distribution curves are depicted in Fig. S2. The detailed values of the specific area and the porosities are shown in Table 3. The SAPO-18 precursor presents a typical type-I isotherm, in accordance with its predominant micropore distribution. The BET surface area and the micropore volume calculated by t-plot method are 680 m² g⁻¹ and 0.28 cm³ g⁻¹, respectively, evidencing the good crystallinity of SAPO-18 precursor. The pore size distribution derived from mercury intrusion porosimetry are shown in Fig. 2. Macropores with size over 300 nm could be observed, which might come from the stacking voids between the crystals.

After TEAOH treatment, the samples present an increased N_2 uptake

Table 2
The bulk and surface compositions of SAPO-18 precursor and products after alkali and acid treatment.

Sample	Product composition	
	Bulk (XRF)	Surface (XPS)
SP18-P	$Si_{0.105}Al_{0.474}P_{0.421}$	$Si_{0.087}Al_{0.449}P_{0.464}$
SP18-TEAOH-0.1	$Si_{0.100}Al_{0.476}P_{0.424}$	$Si_{0.083}Al_{0.460}P_{0.457}$
SP18-TEAOH-0.2	$Si_{0.102}Al_{0.475}P_{0.423}$	$Si_{0.089}Al_{0.444}P_{0.467}$
SP18-NaOH-0.1	$Si_{0.103}Al_{0.500}P_{0.397}$	$Si_{0.081}Al_{0.468}P_{0.451}$
SP18-NaOH-0.4	$Si_{0.111}Al_{0.519}P_{0.370}$	$Si_{0.107}Al_{0.549}P_{0.344}$
SP18-$H_2C_2O_4$-0.1	$Si_{0.080}Al_{0.477}P_{0.443}$	$Si_{0.040}Al_{0.461}P_{0.499}$
SP18-$H_2C_2O_4$-0.2	$Si_{0.034}Al_{0.492}P_{0.474}$	$Si_{0.020}Al_{0.457}P_{0.523}$
SP18-HCl-0.1	$Si_{0.091}Al_{0.474}P_{0.435}$	–
SP18-HCl-0.2	$Si_{0.084}Al_{0.473}P_{0.443}$	–

Table 3
Textural properties of samples.

Sample	S_{BET}[a] (m² g⁻¹)	S_{mic}[b] (m² g⁻¹)	S_{Ext}[c] (m² g⁻¹)	V_{mic}[d] (cm³ g⁻¹)	V_{meso}[e] (cm³ g⁻¹)
SP18-P	680	601	79	0.28	0.07
SP18-TEAOH-0.1	668	588	80	0.27	0.17
SP18-TEAOH-0.2	688	591	96	0.27	0.20
SP18-NaOH-0.1	589	482	92	0.22	0.11
SP18-NaOH-0.2	387	303	84	0.14	0.12
SP18-$H_2C_2O_4$-0.05	623	534	89	0.25	0.09
SP18-$H_2C_2O_4$-0.1	564	476	88	0.22	0.11
SP18-HCl-0.1	628	548	80	0.26	0.09
SP18-HCl-0.2	622	537	85	0.25	0.11

[a] BET surface area.
[b] t-Plot micropore surface area.
[c] t-Plot external surface area.
[d] t-Plot micropore volume.
[e] BJH adsorption volume.

with simultaneous occurrence of hysteria loop in relative pressure range between 0.8 and 0.99, showing the creation of large quantities of meso- and macroporosities. The BJH pore size distribution curves evidence the presence of meso/macropores with the size of 10–100 nm (centering at 20 nm). This is also in good agreement with the mercury intrusion result, which demonstrates the rich existence of mesopores of 10–30 nm. Meanwhile, the BET surface area and micropore volume of the samples are well-preserved, certifying the good stability of the micropores under TEAOH treatment. In contrast, the micropore system is damaged to some extent after NaOH treatment. The micropore volume and surface area decreased by 20% and 50% for SP18-NaOH-0.1 and SP18-NaOH-0.2, respectively. The external surface area (92 m² g⁻¹) and mesopore volume (0.11 cm³g⁻¹) are slightly increased comparing to the parent SAPO-18 precursor, corresponding to the creation of hierarchical porosities. In summary, both organic and inorganic alkaline treatment were able to introduce meso- and macropores into the SAPO-18 crystals. The TEAOH alkaline treatment could well preserve the micro-structure during the creation of hierarchical porosity. The treatment in inorganic NaOH solution only introduce small amount of mesopores and would seriously damage the micropore system simultaneously.

The N_2 physical adsorption results of the samples obtained by acid treatment were also examined (Fig. S3). Compared with TEAOH-treated samples, the generated mesopores (10–50 nm) are relatively sparse in HCl-treated samples, as evidenced by the limited increase of mesopore volume. The mercury intrusion results in Fig. 2 also show that although sample SP18-HCl-0.1 possesses a pore distribution peak in the range of 5–200 nm, the peak intensity is rather weak, implying that the amount of generated pores is few. However, for sample SP18-HCl-0.2, obvious macropores in the range of 100–200 nm can be observed from the pore size distribution from mercury porosimetry analyses, implying that higher HCl concentration facilitates the enhancement of hierarchical porosities. The specific surface area and micropore volume of the HCl-treated samples are all well preserved. For sample SP18-$H_2C_2O_4$-0.1 treated in 0.1 M oxalic acid, the framework structure was significantly damaged, evidenced by the textural parameters listed in Table 3, indicating that HCl acid solution had a milder interaction with the precursor than $H_2C_2O_4$ acid, and could better preserve the micropores and crystallinity. However, it is noted that the number of meso/macropores
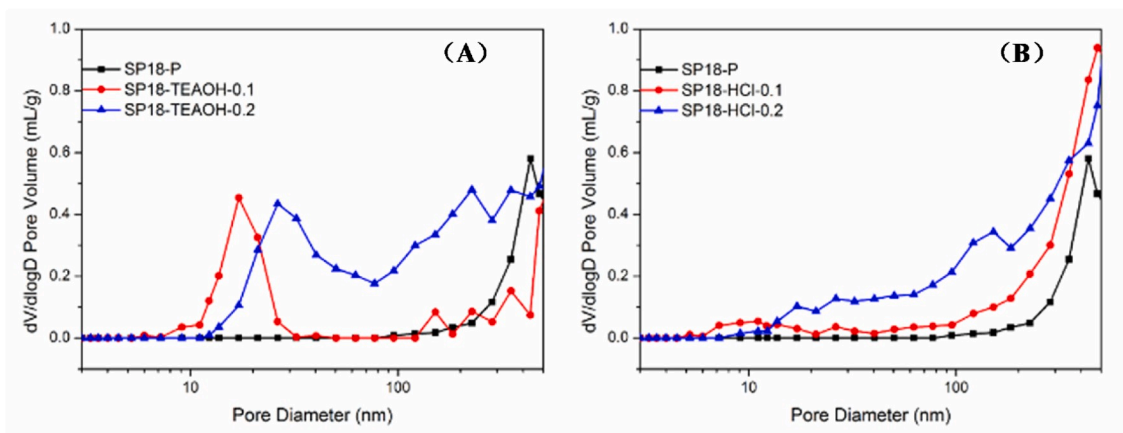
Fig. 2. Pore size distributions of SAPO-18 precursor and products after alkaline (A) and acid treatments (B) measured by mercury intrusion porosimetry.

introduced in the crystals by HCl treatment is smaller and the pore size distribution tends to be wider than the TEAOH-treated samples.

3.5. ^{29}Si, ^{27}Al and ^{31}P MAS NMR

The ^{29}Si MAS NMR spectra of the samples are shown in Fig. 3. Five resonance signals at around −91.5, −95, −100, −105 and −87 ppm could be discerned for SAPO-18 precursor. The signals located in the range of −91.5 to −100 ppm are attributed to the Si(4Al), Si(3Al), Si(2Al), Si(1Al) and Si(0Al) species [23,24]. The peak at −87 ppm comes from Si species with hydroxyl attachment in the defect sites, the possible coordination status of which is Si(OAl)(OSi)$_2$(OH) or Si(OAl)(OSi)(OH)$_2$ [25,26]. The strong intensity of the resonance at −91.5 ppm suggests the predominant occupation of Si(4Al) species in the precursor. For SP18-TEAOH-0.2, the intensities of peaks from −95 to −110 ppm drop, whereas the signal at −87 ppm increases, which suggest the removal of Si species in Si islands and the creation of more defect sites upon TEAOH treatment. The resonance at −91.5 ppm shows less variation, implying that the Si species in the form of Si(4Al) is relatively stable in the TEAOH solution. In the alkaline solution, AlO$_4^-$ in the SAPO framework can effectively prevent the attack of OH$^-$, thereby providing protection to the surrounding framework atoms. Therefore, the Si(4Al) species tetra-coordinated by four AlO$_4^-$ groups has the highest stability in the alkaline solution. In contrast, Si species located inside the Si islands, especially in the center of Si islands, are vulnerable to OH$^-$ attack and preferentially extracted from the framework due to the lack of protection. The low stability of Si islands is more obviously revealed by the ^{29}Si

MAS NMR result of SP18-NaOH-0.4. The resonances from −95 to −110 ppm totally disappeared after treatment in NaOH solution, suggesting the complete dissolution of Si island species. In contrast, Si(4Al) species, instead of Si islands, are more severely extracted for sample SP18-H$_2$C$_2$O$_4$-0.2, reflecting the different stability order of Si species in acid solution. In the acid solution, the negative AlO$_4^-$ in the SAPO framework is prone to attacks by H$^+$. Therefore, the stability of Si(4Al) species surrounded by four AlO$_4^-$ is inferior to other Si species. For sample SP18-HCl-0.2, its ^{29}Si spectrum is not significantly different from that of the precursor, which verifies again the milder interaction between HCl acid and SAPO-18 precursor.

The ^{27}Al MAS NMR spectra of the SAPO-18 precursor and the products after acid/alkaline treatment are shown in Fig. 4. Two resonance peaks at 39 and 11 ppm could be observed for the precursor. The peak at 39 ppm is due to the framework tetrahedral Al species [27]. The signal at 11 ppm arises from penta-coordinated Al species, which is formed by interaction of water or template molecule to the framework Al. After TEAOH treatment, the coordination environment of Al species finds no obvious change, showing the predominant tetra-coordinated Al environment is well preserved. For sample SP18-NaOH-0.4, the peak at 39 ppm is almost completely eroded, implying that most of the framework Al species are extracted from the framework position after treatment in 0.4 M NaOH solution. Two new broad resonances centered around 70 and -5 ppm were observed, corresponding to the extracted Al species in the form of amorphous aluminosilicate or aluminophosphate compound. After treatment in HCl solution, a new peak at −10 ppm was observed, due to the occurrence of extra-framework hexa-coordinated Al
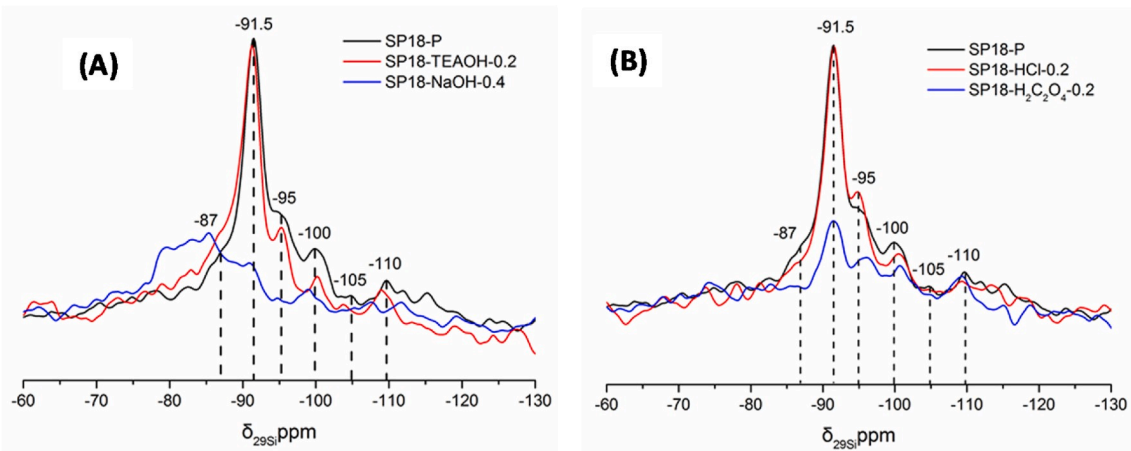
Fig. 3. ^{29}Si MAS NMR spectra of SAPO-18 precursor and products after alkaline (A) and acid treatments (B).
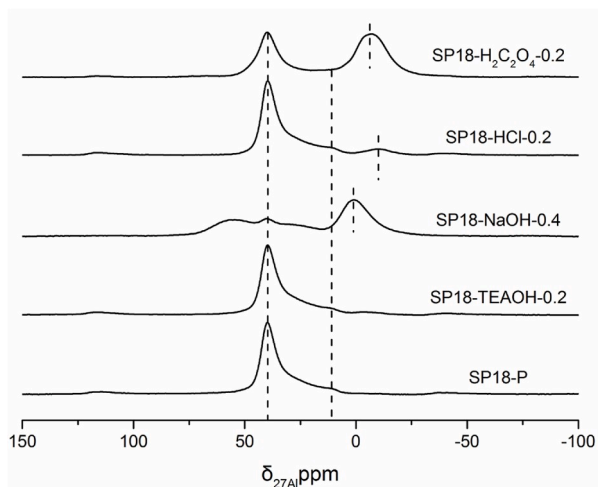
Fig. 4. ^{27}Al MAS NMR spectra of SAPO-18 precursor and products after alkaline and acid treatments.

species [24]. This signal becomes more obvious for sample SP18-H$_2$C$_2$O$_4$-0.2, suggesting that H$_2$C$_2$O$_4$ possesses stronger ability to extract the framework Al species than HCl acid.

Fig. 5 presents the ^{31}P MAS NMR spectra of the samples. A resonance peak at −29 ppm, ascribed to the framework P (4Al) species, dominates the spectrum of the SAPO-18 precursor. Besides, a small resonance signal could be observed at −20 ppm, which could be attributed to the small quantities of inadequate condensed P(OAl)$_x$ (OH)$_y$ species located in the defect sites. The spectra for samples SP18-TEAOH-0.2 and SP18-HCl-0.2 show no big difference comparing to the parent sample, corresponding to the well-preserved crystallinity of the two samples. For SP18-NaOH-0.4 and SP18-H$_2$C$_2$O$_4$-0.2, the peak at −29 ppm is both severely deteriorated, consistent with the removal of large quantities of tetra-coordinated P species from the framework.

3.6. Mechanisms for the acid/alkaline treatment of SAPO-18

In principle, the preparation of hierarchical molecular sieves in both acid and alkaline solutions is achieved by dissolving the regions with poor stability in the precursor crystals. And the distribution of the less stable species, which is closely related to the elemental compositions and the number of defect sites, is key to the creation of desired meso/macropores [28–31]. For SAPO molecular sieves, the PO$_4^+$ species rich in
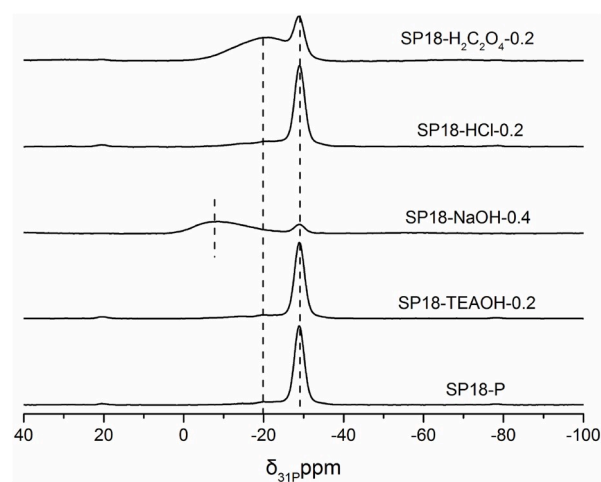
Fig. 5. ^{31}P MAS NMR spectra of SAPO-18 precursor and products after alkaline and acid treatments.

the framework is vulnerable to the attacks of the negatively charged OH$^-$ species in the alkaline solutions. If these attacks happen in an uncontrolled manner, like in the case of NaOH solution of 0.4 mol/L, the P (4Al) species would be preferentially removed and the framework is easily destroyed. In contrast, since the mobility of the OH$^-$ is limited by the bulkier organic counter cations in the TEAOH medium, preferential dissolution occurs surrounding the defect sites in a controlled manner. The microporous framework is consequently well preserved together with its elemental compositions and local atomic coordination environments. The process of hierarchical SAPO-18 preparation in TEAOH solution could be discerned as a defect-mediated process. Firstly, the TEAOH solution interacts with the defected interfaces between the intergrown crystalline domains and creates channels leading to the inside of the crystals; TEAOH molecules diffuse into the crystals through those channels and interact with the internal defects of SAPO-18 crystals; new meso/macropores are created inside the crystals due to dissolution and removal of the defected zone.

After acid treatment in H$_2$C$_2$O$_4$ medium, the Si content of the product decreases significantly (Table 2), indicating that besides the defect zone, the Si atoms located in Si(4Al) regions are preferentially attacked/removed by the H$^+$ cations. Most of the neighboring Al atoms remained in the framework due to the protection of P-O-Al bond. Terminal Al species with OH group is hence created, which is congruent with the ^{27}Al NMR result. The stability of different bonds in H$_2$C$_2$O$_4$ medium can be expressed as follows: Si-O-Si > Al-O-P > Si-O-Al [21]. Under HCl leaching, the Si content of the sample also decreases, but the extent of decline is inferior to that in H$_2$C$_2$O$_4$ medium. This is consistent with the insignificant variation of its Si environment as reflected in the ^{29}Si MAS NMR spectra, suggesting that the chance of defect-induced dissolution in HCl solution is higher than in the H$_2$C$_2$O$_4$ medium. In summary, both the defect-induced and element-mediated dissolutions contribute to the creation of larger pores and more pronounced dissolution of the central part of the SAPO-18 crystals in the acid medium. (Fig. 1).

According to the variation of the physio-chemical properties of SAPO-18 before and after alkaline/acid treatment, an in-depth understanding of the crystallization process of SAPO-18 could be achieved. In the TEAOH solution, the creation of the hierarchical pores is initiated around the defected zones located at the boundaries of the intergrown crystallites. The generated hierarchical pores had radiated shape pointing from the surface to the center of the crystals. It suggests that the twinning growth of the crystallites in the crystallization process proceeds in an ordered way to some extent, leading to the preferential arrangements of twinning boundaries (pointing to the center of the crystals). In both alkaline and acid treatments, the central part of the sample is more severely dissolved, evidencing the enriched defects in the center of crystals. It is speculated that the crystallization of SAPO-18 in the early stages may also proceed by an oriented nanoparticle attachment mechanism as proposed by Rimer et al. [32], generating enriched defect distribution inside the crystal cores.

3.7. Catalytic performance

The model alkylation reaction of benzene with benzene alcohol (BA) is selected to evaluate the catalytic performance of the hierarchical SAPO-18 via acid/alkaline leaching (Fig. 6). In this reaction, diphenylmethane (DPB), an important intermediate for pharmacy and fine chemicals, is the desired product. Dibenzyl ether (DBE) and dibenzyl benzene are by-products. Since the dimension of the reagent benzene or benzene alcohol is larger than the pore opening of SAPO-18, the reaction could only happen on the external surface or inside the created hierarchical channels. For the SAPO-18 precursor, the conversion of benzene alcohol is calculated to be around 25%, and the selectivity towards DPM is lower than 70%. For SP18-TEAOH-0.2 treated in TEAOH solution, the catalytic performance is significantly improved, with a BA conversion of 95.5% and DPM selectivity of 83.5%. These improvements could be attributed to the increase of external surface area and the creation of
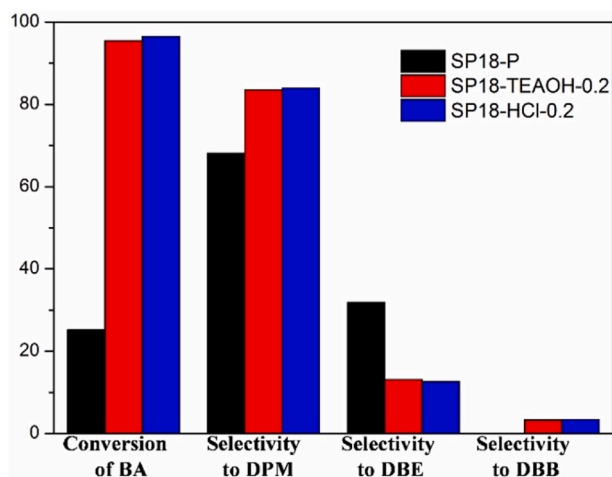
Fig. 6. Results of alkylation of benzene with benzyl alcohol (BA) over the samples. Reaction conditions: catalyst weight = 250 mg, T = 170 °C, t = 1 h.

Fig. 7. NH$_3$-TPD profiles of SAPO-18 precursor and products after alkaline and acid treatments.

hierarchical porosity well connected to the external surface. For SP18-HCl-0.2 after acid treatment, its catalytic performance is even slightly better than SP18-TEAOH-0.2. Considering the fact that the mesopore volume of SP18-HCl-0.2 is inferior to that of SP18-TEAOH-0.2, it is speculated that the improvement of catalytic performance on SP18-HCl-0.2 may come from the creation of more hydroxyl groups and surface acid sites after HCl treatment. This is supported by the NH$_3$-TPD results of the samples. As shown in Fig. 7, SP18-P and SP18-TEAOH-0.2 have similar acid concentrations and distributions, whereas SP18-HCl-0.2 possesses larger quantities of weak acid sites.

4. Conclusions

SAPO-18 molecular sieve with hierarchical pores were prepared for the first time by alkaline and acid treatments. It is found that the use of TEAOH solution could introduce a large number of mesopores in the crystals without significantly changing the composition and acidity of the sample. Preferential dissolution occurs surrounding the defect sites in a controlled manner. In acidic medium, besides the defect-induced dissolution, selective dissolution of the Si-O-Al domains occurs. Both defect-induced and element-mediated dissolutions contribute to the generation of hierarchical SAPO-18 with relatively large quantities of macropores. Based on the variation of the physio-chemical properties of SAPO-18 before and after alkaline/acid treatment, it is inferred that the formation of SAPO-18 may proceed by oriented nano-particle attachment in the early crystallization stage. The twinning and intergrowth of crystallites occurs in an ordered way, leading to the ordered arrangement of the crystallite boundaries or interfaces. The hierarchical SAPO-18 sample exhibits excellent catalytic reaction performance in the liquid phase benzylation reaction of benzene and benzyl alcohol due to its large external specific surface area and mesoporous pore volume.

Declaration of competing interest

There are no conflicts to declare.

CRediT authorship contribution statement

Dong Fan: Writing - original draft, Writing - review & editing, Methodology, Formal analysis. **Yuyan Qiao:** Methodology, Investigation, Visualization, Formal analysis. **Kaipeng Cao:** Investigation. **Lijing Sun:** Software. **Shutao Xu:** Investigation. **Peng Tian:** Supervision, Writing - review & editing, Methodology, Conceptualization. **Zhongmin Liu:** Supervision, Writing - review & editing, Methodology, Conceptualization.
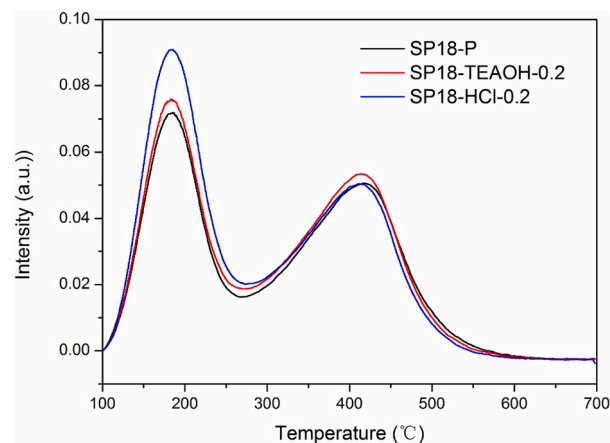
Appendix A. Supplementary data

Supplementary data to this article can be found online at https://doi.org/10.1016/j.micromeso.2020.110156.

References

[1] Z.P. Wang, J.H. Yu, R.R. Xu, Needs and trends in rational synthesis of zeolitic materials, Chem. Soc. Rev. 41 (5) (2012) 1729–1741.

[2] B.M. Weckhuysen, J.H. Yu, Recent advances in zeolite chemistry and catalysis, Chem. Soc. Rev. 44 (20) (2015) 7022–7024.

[3] Y. Li, J.H. Yu, New stories of zeolite structures: their descriptions, determinations, predictions, and evaluations, Chem. Rev. 114 (14) (2014) 7268–7316.

[4] A. Corma, Inorganic solid acids and their use in acid-catalyzed hydrocarbon reactions, Chem. Rev. 95 (3) (1995) 559–614.

[5] W. Schwieger, A.G. Machoke, T. Weissenberger, A. Inayat, T. Selvam, M. Klumpp, A. Inayat, Hierarchy concepts: classification and preparation strategies for zeolite containing materials with hierarchical porosity, Chem. Soc. Rev. 45 (12) (2016) 3353–3376.

[6] V. Valtchev, G. Majano, S. Mintova, J. Perez-Ramirez, Tailored crystalline microporous materials by post-synthesis modification, Chem. Soc. Rev. 42 (1) (2013) 263–290.

[7] X.C. Jia, W. Khan, Z.J. Wu, J. Choi, A.C.K. Yip, Modern synthesis strategies for hierarchical zeolites: bottom-up versus top-down strategies, Adv. Powder Technol. 30 (3) (2019) 467–484.

[8] T. Okubo, Top-down and bottom-up approaches to nanosized and hierarchical zeolites, Abstr. Pap. Am. Chem. Soc. 252 (2016).

[9] M. Klumpp, L.T. Zeng, S.A. Al-Thabaiti, A.P. Weber, W. Schwieger, Building concept inspired by raspberries: from microporous zeolite nanocrystals to hierarchically porous assemblies, Microporous Mesoporous Mater. 229 (2016) 155–165.

[10] C.J.H. Jacobsen, C. Madsen, J. Houzvicka, I. Schmidt, A. Carlsson, Mesoporous zeolite single crystals, J. Am. Chem. Soc. 122 (29) (2000) 7116–7117.

[11] P.F. Wu, M. Yang, W.N. Zhang, S.T. Xu, P. Guo, P. Tian, Z.M. Liu, Synthesis of SAPO-34 nanoaggregates with the assistance of an inexpensive three-in-one non-surfactant organosilane, Chem. Commun. 53 (36) (2017) 4985–4988.

[12] P.F. Wu, M. Yang, L.J. Sun, S. Zeng, S.T. Xu, P. Tian, Z.M. Liu, Synthesis of nanosized SAPO-34 with the assistance of bifunctional amine and seeds, Chem. Commun. 54 (79) (2018) 11160–11163.

[13] Y.Y. Yuan, P. Tian, M. Yang, D. Fan, L.Y. Wang, S.T. Xu, C. Wang, D.H. Wang, Y. Yang, Z.M. Liu, Synthesis of hierarchical beta zeolite by using a bifunctional cationic polymer and the improved catalytic performance, RSC Adv. 5 (13) (2015) 9852–9860.

[14] Y.Y. Yuan, L.Y. Wang, H.C. Liu, P. Tian, M. Yang, S.T. Xu, Z.M. Liu, Facile preparation of nanocrystal-assembled hierarchical mordenite zeolites with remarkable catalytic performance, Chin. J. Catal. 36 (11) (2015) 1910–1919.

[15] S. Lopez-Orozco, A. Inayat, A. Schwab, T. Selvam, W. Schwieger, Zeolitic materials with hierarchical porous structures, Adv. Mater. 23 (22–23) (2011) 2602–2615.

[16] M. Bjorgen, F. Joensen, M.S. Holm, U. Olsbye, K.P. Lillerud, S. Svelle, Methanol to gasoline over zeolite H-ZSM-5: improved catalyst performance by treatment with NaOH, Appl. Catal. Gen. 345 (1) (2008) 43–50.

[17] J.C. Groen, W. Zhu, S. Brouwer, S.J. Huynink, F. Kapteijn, J.A. Moulijn, J. Perez-Ramirez, Direct demonstration of enhanced diffusion in mesoporous ZSM-5 zeolite obtained via controlled desilication, J. Am. Chem. Soc. 129 (2) (2007) 355–360.

[18] J.C. Groen, J.A. Moulijn, J. Perez-Ramirez, Desilication: on the controlled generation of mesoporosity in MFI zeolites, J. Mater. Chem. 16 (22) (2006) 2121–2131.

[19] J.C. Groen, L.A.A. Peffer, J.A. Moulijn, J. Perez-Ramirez, On the introduction of intracrystalline mesoporosity in zeolites upon desilication in alkaline medium, Microporous Mesoporous Mater. 69 (1–2) (2004) 29–34.

[20] J.C. Groen, T. Sano, J.A. Moulijn, J. Perez-Ramirez, Alkaline-mediated mesoporous mordenite zeolites for acid-catalyzed conversions, J. Catal. 251 (1) (2007) 21–27.

[21] D. Verboekend, M. Milina, J. Perez-Ramirez, Hierarchical silicoaluminophosphates by postsynthetic modification: influence of topology, composition, and silicon distribution, Chem. Mater. 26 (15) (2014) 4552–4562.

[22] Y.Y. Qiao, M. Yang, B.B. Gao, L.Y. Wang, P. Tian, S.T. Xu, Z.M. Liu, Creation of hollow SAPO-34 single crystals via alkaline or acid etching, Chem. Commun. 52 (33) (2016) 5718–5721.

[23] D. Fan, P. Tian, X. Su, Y.Y. Yuan, D.H. Wang, C. Wang, M. Yang, L.Y. Wang, S. T. Xu, Z.M. Liu, Aminothermal synthesis of CHA-type SAPO molecular sieves and their catalytic performance in methanol to olefins (MTO) reaction, J. Mater. Chem. 1 (45) (2013) 14206–14213.

[24] C.S. Blackwell, R.L. Patton, Solid-state nmr of silicoaluminophosphate molecular-sieves and aluminophosphate materials, J. Phys. Chem. 92 (13) (1988) 3965–3970.

[25] L. Zhang, J. Bates, D.H. Chen, H.Y. Nie, Y.N. Huang, Investigations of formation of molecular sieve SAPO-34, J. Phys. Chem. C 115 (45) (2011) 22309–22319.

[26] B.H. Chen, Y. Huang, Examining the self-assembly of microporous material AlPO (4)-11 by dry-gel conversion, J. Phys. Chem. C 111 (42) (2007) 15236–15243.

[27] D. Fan, P. Tian, S.T. Xu, Q.H. Xia, X. Su, L. Zhang, Y. Zhang, Y.L. He, Z.M. Liu, A novel solvothermal approach to synthesize SAPO molecular sieves using organic amines as the solvent and template, J. Mater. Chem. 22 (14) (2012) 6568–6574.

[28] Z.X. Qin, G. Melinte, J.P. Gilson, M. Jaber, K. Bozhilov, P. Boullay, S. Mintova, O. Ersen, V. Valtchev, The mosaic structure of zeolite crystals, Angew. Chem. Int. Ed. 55 (48) (2016) 15049–15052.

[29] Z. Qin, L. Lakiss, J.P. Gilson, K. Thomas, J.M. Goupil, C. Fernandez, V. Valtchev, Chemical equilibrium controlled etching of MFI-type zeolite and its influence on zeolite structure, acidity, and catalytic activity, Chem. Mater. 25 (14) (2013) 2759–2766.

[30] Z.X. Qin, J.P. Gilson, V. Valtchev, Mesoporous zeolites by fluoride etching, Curr. Opin. Chem. Eng. 8 (2015) 1–6.

[31] X.X. Chen, A. Vicente, Z.X. Qin, V. Ruaux, J.P. Gilson, V. Valtchev, The preparation of hierarchical SAPO-34 crystals via post-synthesis fluoride etching, Chem. Commun. 52 (17) (2016) 3512–3515.

[32] A.I. Lupulescu, J.D. Rimer, In situ imaging of silicalite-1 surface growth reveals the mechanism of crystallization, Science 344 (6185) (2014) 729–732.